Observation of Defect Distribution in H Ion Implanted Silicon

Hイオン注入されたシリコンの欠陥分布観察

H. IWATA[1)], M. TAKAGI[2)], Y. TOKUDA[3)] and T. IMURA[1)]

岩田 博之[1)],　高木 誠[2)],　徳田 豊[3)],　井村 徹[1)]

Abstract: The fundamental mechanism of the hydrogen exfoliation phenomenon that occurs at the damaged layer in H ion implanted silicon was investigated. A damaged layer formed by high-dose hydrogen implantation in a silicon wafer was observed by cross sectional transmission electron microscopy (XTEM), and (100) defects and (111) defects were visible. Density and size of the defects in the damaged layer were analyzed quantitatively. Although the density and size of (100) defects are almost twice those of (111) defects, the density of (111) defects in the deeper area is greater than the density of (100) defects. Neither the densities nor size of either (100) or (111) defects have any relation with implantation dose in the dose range from 5.0×10^{16} to 8.0×10^{16} [Hcm^{-2}]. The sizes of (111) defects in the deeper area approach a certain size (about 10nm), because of their partial combination with (100) defects.

1. Introduction

The behavior of hydrogen in solid materials remains a matter of everlasting interest in materials engineering. Hydrogen in silicon plays an important role in the semiconductive behavior of silicon, such as, for example, passivation of the electrical properties of shallow acceptors and donors. Blistering, flaking and exfoliation phenomena caused by high-dose ion implantation have long been investigated. SOI (silicon on insulator) fabrication has become an attractive technology for low power, low voltage and high-speed electronics. Much attention has been given to the hydrogen exfoliation method introduced by Bruel. [1] in comparison with other SOI fabrication techniques. This method involves the micro slicing process of silicon by high-dose hydrogen implantation and has advantages of greater uniformity of thickness of the surface layer and crystal quality than other processes [1,2]. Although this unique and useful process has been extensively developed in industrial applications during the past few years, the fundamental phenomenon and the underlying mechanism are still not completely understood [3].

Defect structures lying in {100} and {111} planes have been observed in the damaged layer of hydrogen-implanted silicon [4]. The local vibration corresponding to the bond-stretching mode of Si-H was investigated by Raman and infrared spectroscopy [5], namely Si-Si bonds along {111} plane were broken by hydrogen

1)　愛知工業大学　総合技術研究所（豊田市）
2)　愛知工業大学　機械工学科（豊田市）
3)　愛知工業大学　電子工学科（豊田市）

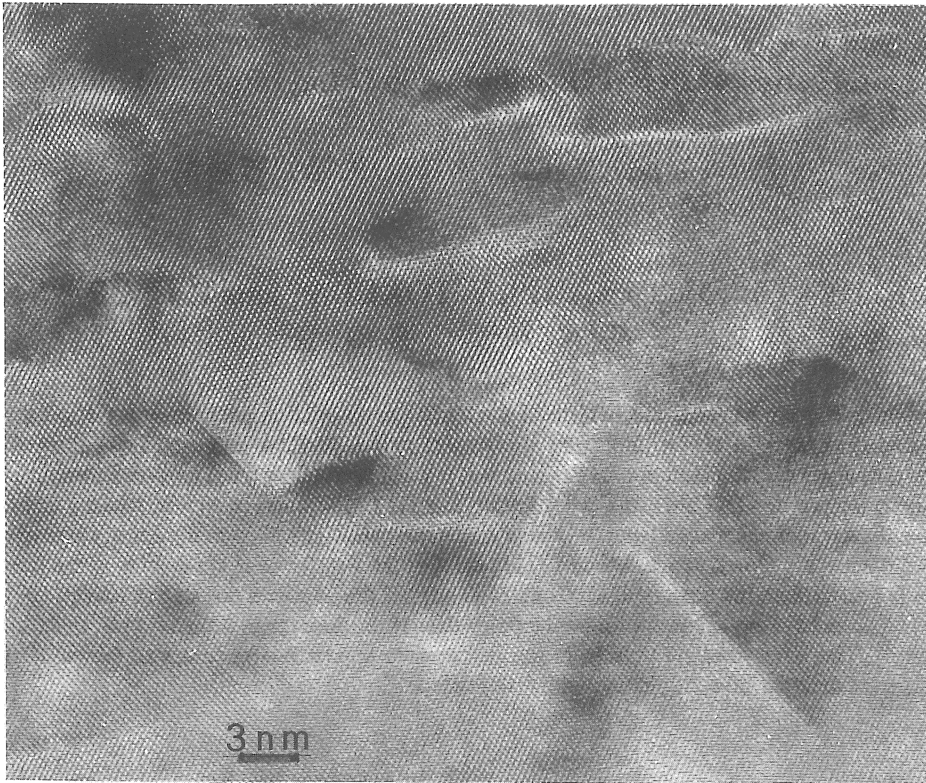

Fig. 1 XTEM bright field image of the damaged layer in Si implanted with 8×10^{16} H/cm^2 after room temperature implantation. 80keV implantation was carried out from top (surface)-to-bottom. The high-resolution image was taken along [110].

implantation and Si-H bonds formed. Muto et al. found that hydrogen induced defects originate with hydrogen-saturated bonds arranged on a (111) plane by using high-resolution transmission electron microscopy (HRTEM) images [6]. They found that the defect contains a high density of gas molecules and that the inside pressure is more than 1GPa. Asper et al. examined the typical distribution of the size of {100} defects, and reported that the size distribution fits a gaussian function. Moreover, a decrease of defect density and on increase in defect size during annealing was reported [7].

Weldon et al. examined the Si-H bond formation using infrared spectroscopy measurement [8], and reported that the trapped hydrogen atoms diffuse and form microcavities filled with H_2 molecules during thermal annealing. The high pressure inside the microcavity becomes the driving force for its expansion and growth, and results in fracture near the peak implantation region. If a bonded wafer is capped on the implanted wafer surface, microcavities grow along (100) plane parallel to that surface during annealing. After all the microcavities are linked together, the bonded wafer pair becomes completely separated along the cavity plane. If no capping layer is present, the microcavities cannot link widely, so that small pieces of cleaved silicon layer

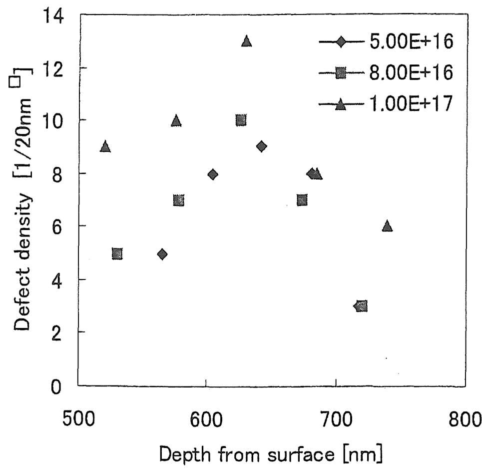

Fig. 2(a). (100) defect density

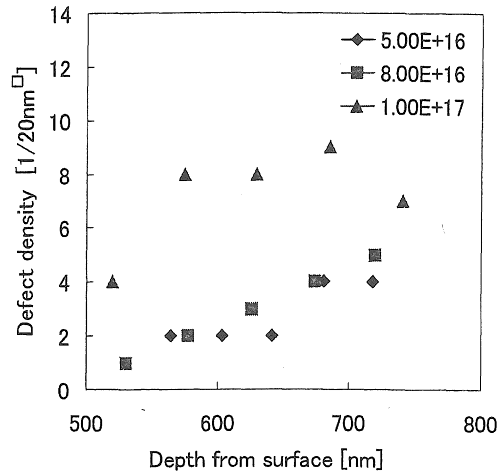

Fig. 2(b). (111) defect density

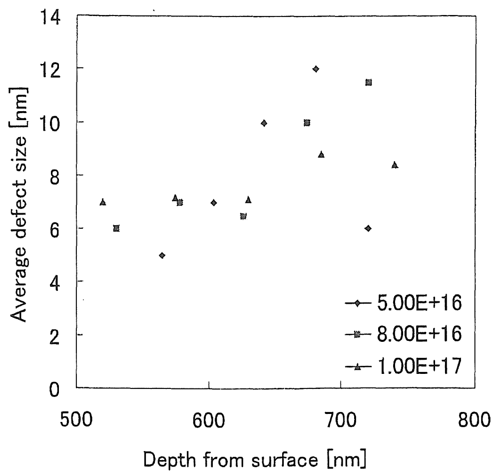

Fig. 3(a). (100) defect size

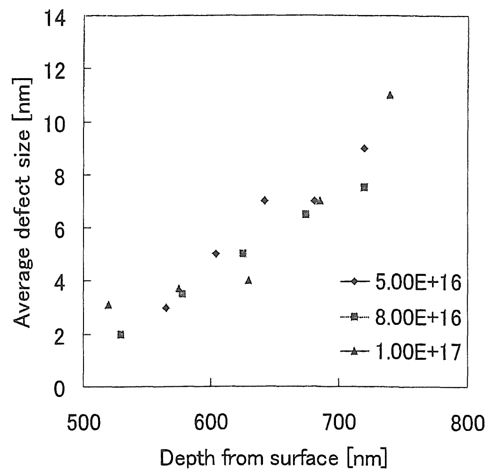

Fig. 3(b). (111) defect size

are obtained. The driving force of this cleavage mechanism is the gas pressure in the microcavities. Generation of blisters causes a thin film to be split from the mass of the material,and thickness of the film is essentially equal to the projection range (Rp).

In this study, defect distributions were examined using cross sectional transmission electron microscopy (XTEM), and the results of quantitative analysis of defect distributions determined . From the depth profile, the reason the exfoliation is obtained along Rp was verified. We attempted to explain the roles of the two kinds of defects in the exfoliation phenomenon.

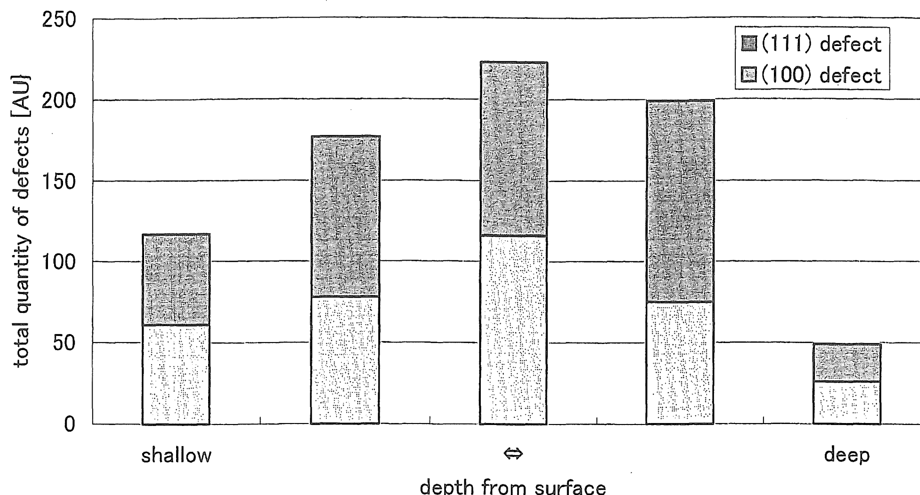

Fig.4. The total quantity of defects calculated from (density) × (the weighted mean average length of defects). (the implantation dose is 8×10^{16} H/cm^2)

2. Experiments

All experiments were performed with p-type CZ-grown (100) silicon. Hydrogen ion implantation was made parallel to the [100] direction of (100) oriented silicon with 80keV energy. The dose ranges are from 5.0 x10^{16} to 8.0x10^{16}Hcm^{-2}. The cross-sectional specimen preparation involved gluing two small pieces face-to-face from a single as implanted sample and mounting them on a 3mm brass pipe. Samples were cut into disks of 3mm diameter and mechanically polished. Then, the disks were dimpled at the center and thinned by argon ion milling. TEM analysis was carried out with a JEM-2010 operated at 200kV.

3. Results and Discussion

The depth of the damaged layer is approximately 500nm below the surface. This depth is in agreement with the result of hydrogen concentration estimated from a secondary ion mass spectroscopy (SIMS) profile. Figure 1 shows the XTEM bright field image taken along [110] of the damaged layer of a Si sample implanted with a 8.0x10^{16}Hcm^{-2} dose. The damaged layer consists of two kinds of defects: (1) (100) defects existing parallel to the surface shown by changing the direction of electron beam in the high resolution TEM and (2) (111) defects shown by changing the direction of the electron beam. Comparing the damaged layer with lower dose implanted samples; the quantities of macroscopic defects have a close correlation with the dosage. Therefore, thickness of the damaged layer is roughly proportional to the implantation dose.

The defects along (100) and (111) seem to be the key defects in the hydrogen

exfoliation phenomenon, because most of them are located at the depth of Rp where exfoliation occurred. Accordingly, (100) and (111) defects were classified into five areas depending on the depth, and their size and density were investigated in detail. The five areas located at equal intervals in the depth direction in the have the same 20nm ×20nm area. Defect sizes are defined by calculating the average diameter of the defects in each area in the high-resolution micrograph taken along the [110] direction, and defect densities are defined as the number of defects counted in each area in this micrograph.

Figure 2 (a) shows the defect density existing along the (100) plane and (b) shows that along the (111) plane; (a) illustrates the density of (100) defects having a peak in the layer at a depth of around 650nm. The depth is in agreement with theoretically estimated Rp value and hydrogen concentration data obtained from the SIMS profile. In contrast, the density of (111) defects has no apparent peak, and becomes higher as the area deepens. The density of (100) defects is relatively higher than that of (111) defects, except in deeper area (over 700 nm deep from surface). In this deeper area of the damaged layer, the density of (111) defects is greater than the density of (100) defects. Densities of neither defects have any relation to the implanted doses used in this experiment.

Figures 3 (a) and (b) show the average defect sizes along (100) and (111), respectively. Defects of both sizes have the same tendency: the defects located in the deeper region are larger in size than those located in the shallower region. The size of (100) defects is almost twice that of (111) defects. The size of (111) defects depends on the relationship with adjoining (100) defects, so that the decrease of (100) defect density in the deeper area induces the increase of (111) defect size. Consequently, the size of (111) defects in the deeper area approaches a certain size of about 10nm. The sizes of both (100) and (111) defects have no relation to the implanted doses used in this experiment. Figure 4 shows the total quantity of defects calculated by multiplying the density and the weighted mean average length of defects. The results verify that the defects have a quantitative peak around Rp. On the other hand, from the literature [4], during annealing, the (100) defect density decreases and the size increases. Moreover, from our annealing experience, the (111) defect density decreased after annealing. The fundamental exfoliation mechanism can be deduced from the results of this study and understood as follows: judging from the fact that defects contain hydrogen gas during thermal annealing, the trapped hydrogen atoms diffuse and segregate around the Rp depth and form microcavities filled with H_2 molecules. The high pressure inside the microcavity becomes the driving force for its expansion and growth. Furthermore, (100) defects obtained by implantation have a tendency to become a way of escape for high-pressure H_2 molecules. Summing up the entire hydrogen movement in the damaged layer, hydrogen in (111) defects diffuses toward (100) defects around Rp. Therefore, the pressure of hydrogen gas leads to the exfoliation, and this is the reason for the exfoliation along Rp.

Acknowledgements

The author would like to thank S. Yamauchi and H. Ohshima, Research Laboratories, Denso Co., Ltd. for their supplies of silicon wafers and SIMS data.

References

[1] M. Bruel, Electronics Letters **31** (1995) 1201
[2] M. Bruel, Nuclear Instrument and Methods B**108** (1996) 313
[3] Q.Y. Tong, R.W. Bower, MRS Bulletin **23** (1998) 40
[4] S.Romani, J.H. Evans, Nuclear Instrument and Methods B**44** (1990) 313
[5] N.M. Johnson, F.A. Ponce, R.A. Street, R.J. Nemanich, Physical Review B **35** (1987) 4166
[6] S. Muto, S. Takeda and M. Hirata, Material Science Forum, **143-147** (1994) 897
[7] B. Asper, M. Bruel, H. Moriceau, C. Maleville, T. Pounmeyrol, A.M. Papon. Microelectronics Engineering **36** (1997) 233
[8] M.K. Weldon, V.E. Marsico, Y.J. Chabal, A. Agarwal, D.J. Eaglesham, J. Sapjeta, W.L. Brown, D.C. Jacobson, Y.Caudano, S.B. Christman and E.E. Chaban, J. Vacuum Science Technology B **15**(1997) 1065

（受理　平成12年３月18日）